

Creep/Fatigue Behavior of Resin Infused Biaxial Glass Fabric Laminates

Daniel D. Samborsky¹, John F. Mandell¹ and David A. Miller²

¹*Department of Chemical and Biological Engineering,*

²*Department of Mechanical and Industrial Engineering,*

Montana State University, Bozeman, MT, 59717, USA

Abstract

This study has explored creep/fatigue effects for infused glass/epoxy biaxial ($\pm 45^\circ$) fabric laminates typical of shell/web areas of wind blades. Loading conditions were cyclic fatigue at R-values 0.1, -1 and 10, as well as tensile and compressive creep. Cyclic stress-strain loops for load and strain control are compared. The results are discussed in terms of the relative creep or cyclic dominance and appropriate fatigue design criteria. Laminates with a low content of 0° unidirectional plies added to the biaxial plies were also briefly studied in terms of the interaction of creeping, softening effects of the biaxial plies on the performance of the 0° plies.

I. Introduction

Wind turbine blade structures typically include significant quantities of biaxial laminates with $\pm 45^\circ$ oriented fibers in the shells and webs, to resist torsion and buckling, and in the root, to build up the thickness. While not considered the primary structure, represented by unidirectional (UD) plies oriented along the blade axis (0°) in spars, the biaxial laminates and plies must perform without significant damage or failure at the strain levels and environments experienced by the blade in service. Edgewise, reversed loading in large blades is carried substantially by the shell, which may contain some fraction of unidirectional plies for this purpose; often, additional unidirectional fabric reinforcement is added at the trailing edge.

The off-axis orientation of the $\pm 45^\circ$ fibers introduces strong material nonlinearity to the static response^{1,2}, as well as significant damage accumulation, creep and strength and stiffness loss prior to total failure in fatigue³⁻⁶. Bending loads produce the highest strains at the outermost fibers, which are usually biaxial fabric in the shell. Thus, the biaxial materials must resist the maximum blade strains under static and fatigue loads without failure or softening enough to reduce the blade stiffness or overload adjacent UD material. Biaxial laminates have received relatively little attention in studies compared with UD and multidirectional (MD) laminates, and creep effects in blade laminates have not been well characterized despite their obvious relevance.

This study has explored the behavior of epoxy resin infused biaxial glass fabrics of three types which vary in structure. S-N fatigue lifetime to total failure (defined later) has been characterized for tension-tension, compression-compression, and reversed loading fatigue ($R = 0.1, 10$ and -1 , respectively, where $R = \min \text{load}/\max \text{load}$ ^{1,2}). Then, concentrating on one typical fabric, a more detailed study of strain accumulation, cyclic stress-strain and residual stress-strain response, stiffness change and creep has been carried out for each R-value.

II. Background

A. Time vs. Cyclic Effects

Blade laminates may be subjected to various combinations of cyclic fatigue loading and static or cyclic creep loading. Most studies have been concerned with cyclic fatigue loading to total failure, primarily with fiber dominated laminates having more than 25% 0° (load direction) fibers. A number of studies have considered creep, creep rupture (sometimes termed static fatigue) and creep/fatigue interactions. Basic treatment of the viscoelastic response can be found in refs. 11-14. Tamuzh, et al.¹⁵ have considered the combined off-axis creep and cyclic fatigue response of glass/polyester laminates. Their findings suggest that cyclic loading results only in a reduction in

stiffness as damage accumulates, but does not affect the viscoelastic response. Mandell and Meier¹⁶ systematically varied the waveform, R-value and frequency (over several decades) to explore creep/fatigue interactions for a fiber dominated 0/90 prepreg glass/epoxy laminate under tensile loading. The results re-plotted as trend lines in Figure 1 indicate the typical scenario for fiber dominated glass laminates: the fatigue lifetime was cycle dominated at longer lifetime, with creep effects playing a significant role at higher loads/shorter lifetimes, and low frequencies. In the high cycle/low stress range of interest for wind blades, creep effects are not expected to play a significant role for fiber dominated laminates.

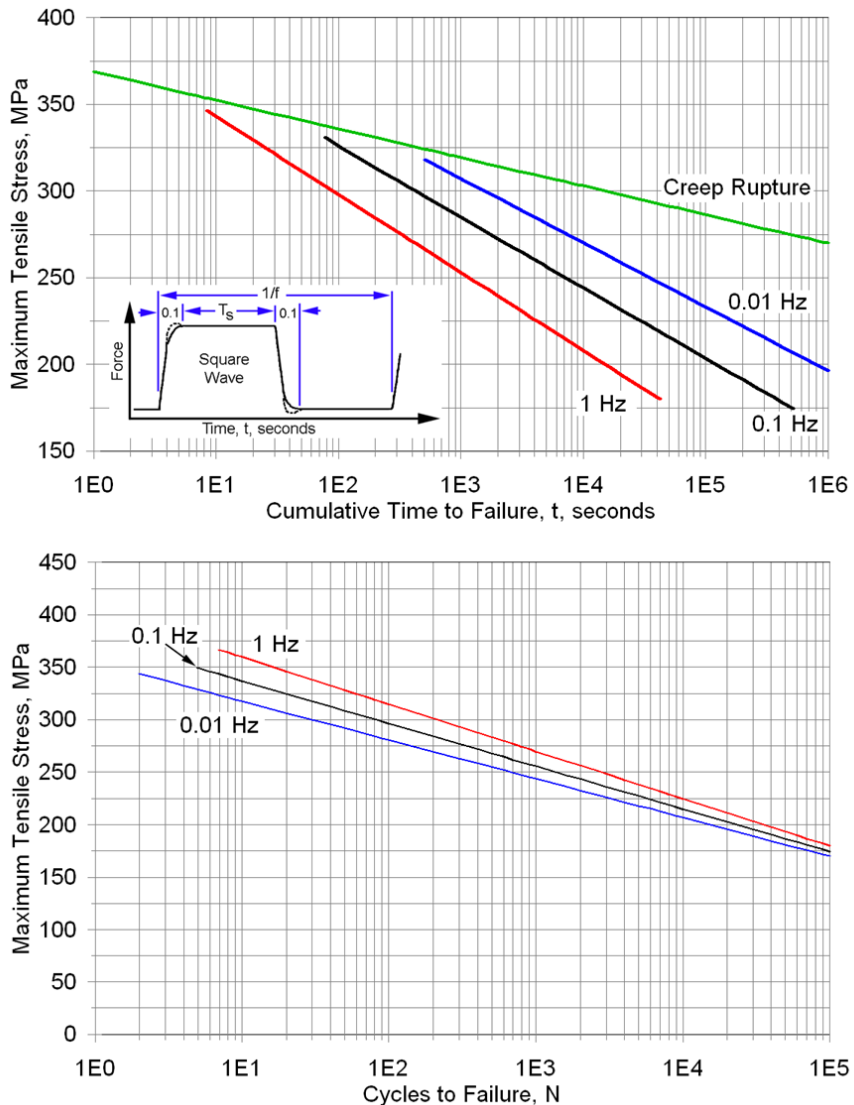


Figure 1. Creep rupture and tensile fatigue trends plotted in terms of cumulative time under load (top) and fatigue cycles (bottom); square wave loading at three frequencies, 0/90 glass/epoxy prepreg laminate (replotted from ref. 16).

Creep rupture and cyclic data under both tensile and compressive loading for multidirectional infused fiber dominated glass/epoxy blade-type laminates reported by Nijssen, et al.¹⁷, shows much lower failure stresses at the same approximate loading time for cyclic loading at $R = 0.1$ and 10, compared with creep rupture, consistent with Figure 1. Frequency effects at higher frequencies with sine wave loading have been reported to be consistent with Figure 1 for infused fiber dominated blade laminates¹⁸. Epaarachchi¹⁹ describes fatigue and creep rupture data for a multidirectional glass/polyester laminate for tensile fatigue loading between $R = 0.5$ and 1.0. Models incorporating both creep rupture and cyclic parameters provided the best fit to the data.

B. Biaxial Fabric Fatigue Behavior

Tensile fatigue SN curves have been reported for a variety of blade materials with $\pm 45^\circ$ construction and epoxy resins, either prepreg or infusion processed. A selection of results from the SNL/MSU/DOE¹⁰ and European OPTIdat²¹ databases are compared in Figure 2. Differences are not great considering the range of materials systems. The backing strands in fabric L result in slightly directional behavior², and the mat backing on fabric M increases the strength and stiffness but reduces the failure strain significantly¹. (Fabrics L and M are included in the present study.) Much of the reported study of $\pm 45^\circ$ blade laminates has involved materials composed of UD fabrics or prepreg plies stacked at $\pm 45^\circ$, rather than commercial biaxial fabrics. While most studies have been limited to uniaxial loading of simple test coupons, multi-axial tension/compression/torsion results have been reported by Kensche⁸ for a $\pm 45^\circ$ UD fabric laminate.

Philippidis and Eliopoulos⁵ provide detailed characterization of both fiber and resin dominated static and fatigue behavior of infused glass/epoxy blade laminates, including stiffness degradation, residual strength and creep effects, and their implementation into a damage progression based code (FADAS). Their treatment is based on individual ply axial, transverse and shear characterization, with the shear response derived from tests of $\pm 45^\circ$ laminates composed of oriented unidirectional fabric plies, similar to the Optimat material MD3, Figure 2.

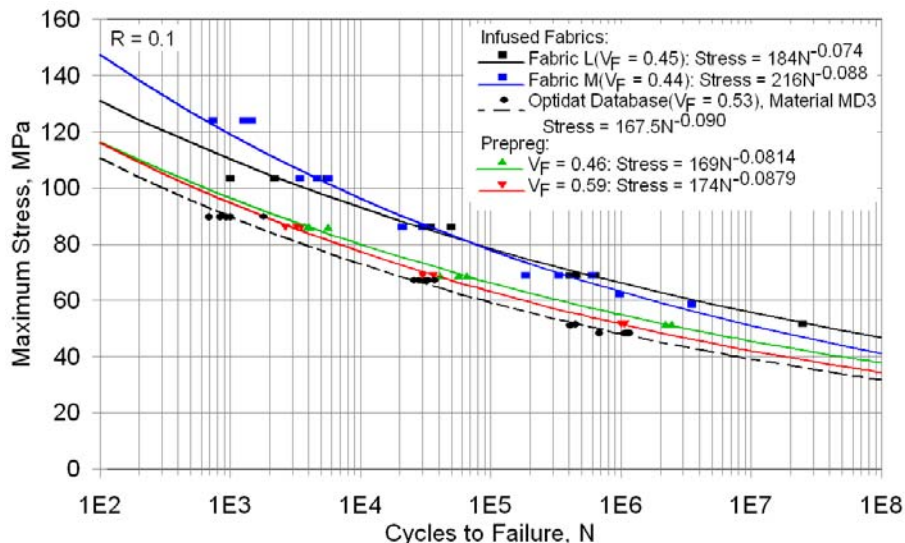


Figure 2. Comparison of literature data^{10,21} for biaxial glass/epoxy infused and prepreg blade laminates in tensile fatigue, R = 0.1.

The effect of resin on biaxial fabric laminates has been explored by Mandell, et al.^{1,9}. Fabric M laminates (Table 1) infused with three different epoxies, two vinyl esters and one polyester showed only moderate effects of resin type on tensile stress-strain and tensile fatigue performance¹. This fabric contains about 27% mat, and behaves in a more fiber dominated or mixed fashion. A similar range of resins with a DB120 biax fabric, which contains no backing strands, showed significantly more variation in strength with resin type⁹. Differences were particularly strong at elevated temperatures and with moisture saturation. Creep rupture data for a wide range of early, low fiber content, fiber dominated and biaxial fabric laminates are available in ref. 9.

III. Experimental Methods

Laminates were resin infusion molded as described in ref. 1. The three constructions of biaxial fabric included in the study are described in Table 1: fabric L contains 2.5% glass strand warp direction backing and fabric M contains 27% content of backing mat¹. The resin was Momentive RIM135/RIMH1366 epoxy, labeled EP-1, widely used in blades. Cure conditions were 24 hrs at 20°C followed by 24 hrs at 90°C (fabrics L and M) or 70°C (fabric P). Laminates used for tensile tests had the configuration $(\pm 45)_{3S}$, about 3.4 mm thick; laminates for compression and reversed loading were $(\pm 45)_{8S}$, about 8.6 mm thick. The fiber volume content for fabric P laminates was about 56% for the tension coupons and 58% for the compression coupons; fabric L and M laminate fiber volume contents were 44 to 45%; a separate panel with fabric P was prepared at 46% to explore possible fiber content effects relative

to the lower contents for fabrics L and M. Thus, fabric P laminates differed significantly in structure, fiber content and cure conditions¹⁰ relative to fabric L and M laminates which were tested at an earlier time¹.

Test coupons (Figure 3) were simple rectangles of constant width with no tabs; compression and reversed loading coupons were thicker and with a shorter gage section to preclude elastic buckling. Coupons were clamped in laterally constrained hydraulic grips as described in ref. 1; test frequencies were kept low to reduce heating: 1 to 4 Hz at $R = 0.1$; 0.5 to 2 Hz for reversed loading and compression. Coupons were conditioned and tests conducted in ambient laboratory air, approximately 20°C and 20 to 30 % RH. Surfaces were fan cooled¹ and surface temperatures rose by less than 10-15°C up to 95% of the lifetime, but then rose more significantly in the final cycles in the failure zone under reversed loading and compression. The failure zone characteristic of $R = -1$ failures (Figure 4) may indicate that the temperature approached the glass transition temperature in that local area; temperatures as high as 70°C were measured. Failure appeared imminent just prior to the rapid temperature rise, so lifetime data may be slightly conservative relative to tests with less temperature rise. Frequency was approximately linearly compensated relative to maximum load. Creep tests ($R = 1.0$) used the fatigue tensile and compression geometries and were continued until the strain rate reached a high level, as described later. Most fatigue tests were run under sine-wave, load control, constant amplitude, at indicated R-values. Additional tests were run under strain control through an extensometer attached to one coupon face. Strain gages on both coupon faces were used to validate extensometer data in selected cases, but the strain gages failed early in the damage progression process. Failures were in the gage section (Figure 3); compression tests were usually terminated just as the failure process began due to excessive strain and distortion (and temperature rise) at total failure. Individual test conditions and results can be found in the current or next annual update of the database¹⁰.

Table 1. Dry fabric construction by weight percent (0° is the warp direction; no 0° fibers)

Fabric Code	Fabric	Weight (g/m ²)	±45°	90°	Stitching	Mat
L	Saertex VU 90079	831	96.8	2.5	0.7	0
M	FMG SX-1708	857	71.1	0	1.9	27.0
P	PPG-Devold DB810-E05	808	99.3	0.1	0.7	0

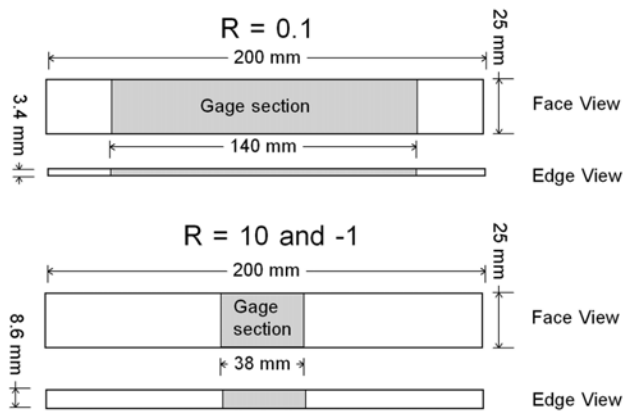


Figure 3. Test coupon geometries, fabric P laminates.

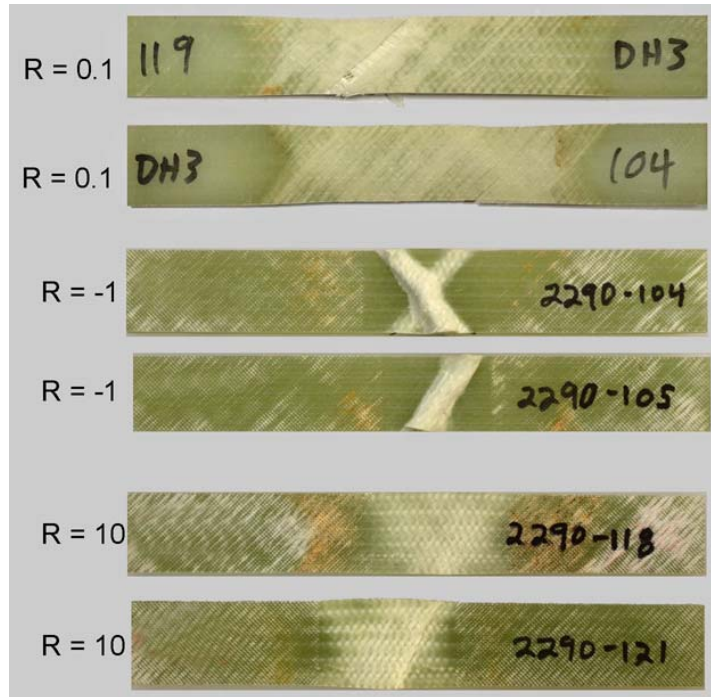


Figure 4. Failed fatigue coupons at indicated R-values, fabric P laminates.

III. Results and Discussion

A. Static Stress-Strain Behavior and Rate Effects

Tensile and compressive stress-strain curves for fabric P laminates are given in Figure 5; the maximum load levels for each fatigue R-value are indicated for reference. The stress-strain response of ± 45 laminates is not only strongly nonlinear, but also very rate sensitive. The curves in Figure 5 were obtained at a relatively slow linear ramp rate of 0.025 mm/s, a typical test standard value. When tested at the typical fatigue average displacement rate, 12.6 mm/s, the tensile maximum load was 50% higher for this material system¹⁰. At the higher fatigue rate, the curves are less nonlinear at the load ranges shown, and strain values would be lower. Fabric M laminates, with random mat backing, showed a corresponding 30% tensile maximum load difference at the two rates¹⁰. As the stress-strain curve becomes significantly nonlinear, or as fatigue cycles increase, damage can be observed to form (Figure 6) and intensify in the laminate.

B. Effects of Fabric and R-value on Fatigue S-N Results

This section presents fatigue S-N results for coupon failure (separation, collapse, or high distortion, Figure 4) under constant force amplitude for the different fabrics and loading conditions. Matrix cracking (Figure 6) is observed during much of the fatigue lifetime before failure, with differences in details for each R-value. In tension (left), R = 0.1, matrix cracks tend to start at coupon edges and progress across the coupon; in reversed loading (center) R = -1, cracking tends to initiate over the fabric stitch lines; and in compression (right), R = 10, cracking and small delaminations are observed between the fabric stitch lines.

A comparison of fatigue S-N curves for laminates based on fabrics L, M and P loaded in the warp direction, and tested at R-values 0.1, -1 and 10 is presented in Figure 7. It was thought that the lower stresses for fabric P may relate to its higher fiber volume content, 56%, compared to the other fabrics, 44-45%. The fabric P data at R = 0.1 fall slightly below the OptiDAT MD3 biaxial laminate which has a similar fiber content (53%) and resin. Tensile fatigue data for a specially prepared panel using fabric P, but with 46% fiber, showed about the same tensile strength and fatigue lifetimes as for the higher fiber content laminates, so fiber content may not play a major role for fabric P laminates in this range. A second factor with fabric P is the absence of significant backing strands relative to the other fabrics (Table 1). The fabric P laminate data fall slightly below the others in Figure 2 (the fabric L and M data were reported in reference 1, and are shown on Figure 2). Finally, the post cure temperature with fabric P was 20°C lower, as noted earlier.

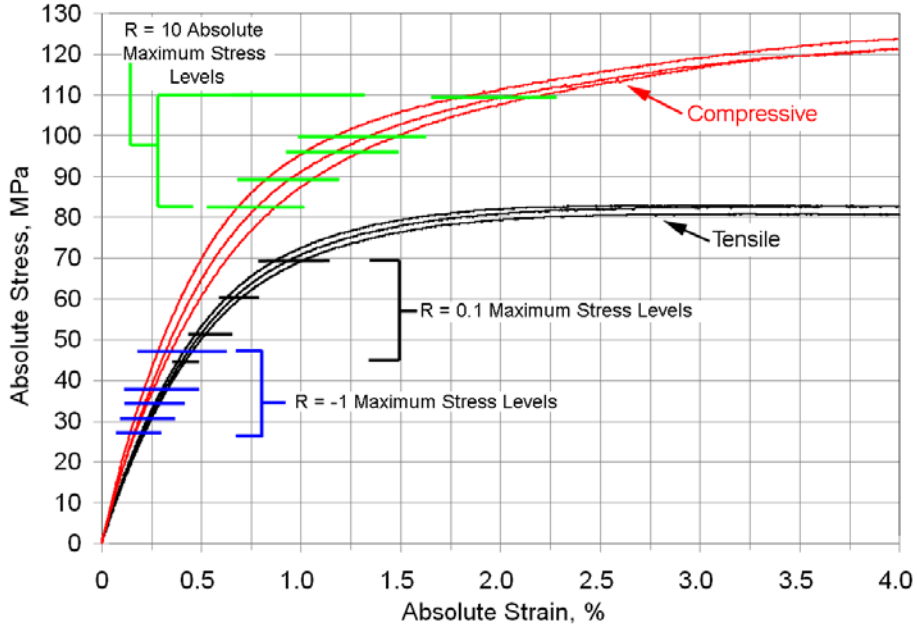


Figure 5. Static stress-strain curves indicating fatigue maximum load levels at each R-value, displacement ramp speed 0.025 mm/s.

Comparing results for different R-values in terms of maximum stress (Figure 8, left), the fatigue stresses are significantly higher for compression compared with tension, contrary to some literature assumptions⁵ and reversed loading is significantly lower, with the same relative trend observed for each of the fabrics in Figure 7. The performance at R = -1 shows a greater drop relative to 0.1 in terms of max stress, than for typical fiber dominated laminates⁹. Fatigue exponents shown on the curve fits indicate S-N trends which are significantly less steep than for many fiber dominated laminates, particularly for fabric P^{1,7}.

The data for different R-values are re-plotted in Figure 8 in terms of stress and the absolute stress amplitude, (max stress – min stress). In these terms, the reversed loading performance is similar to that in compression, and superior to that in tension.

Although biaxial fabrics are used in blades as a stitched unit, their behavior can be more clearly understood by examining the stress field in each ply separately. Standard elastic ply-by-ply laminate analysis²² of ±45° laminates with glass/epoxy ply properties obtained from UD coupons¹, loaded in the axial (0°) direction by a typical applied average stress, σ_x , of 50 MPa in tension or compression, gives the ply coordinate stresses in Table 2. These stresses provide an approximate idea of the nature of the stress state in typical tests, ignoring nonlinearity. (The shear stresses, σ_6 , are identical to those obtained following ASTM test standard D3518, $\sigma_x/2$.) Approximate local stresses at other applied stress levels would change proportionally. Under axial loading in the 0° direction, the results in Table 2 show that a tensile axial load produces transverse tensile (+) stress in each ply, and an in-plane shear stress which is in opposing directions (signs) in the two ply orientations. Transverse compression and opposite shear directions occur under axial compression. In fatigue, resin cracking develops parallel to the fibers (Figure 6). Ultimately, the plies are bonded together by resin as well as stitching, and total separation requires delamination, which is the final mechanism of failure for R = 0.1 (Figure 4).

Table 2. Local ply stresses from classical laminate theory for a (±45)_{ns} glass/epoxy laminate, resulting from an applied axial tensile or compressive stress.

Ply Direction In ±45° Laminate	Applied Stress, σ_x (MPa)	Longitudinal σ_1 (MPa)	Transverse σ_2 (MPa)	Shear σ_6 (MPa)
+45	+50	+47.7	+2.27	-25.0
-45	+50	+47.7	+2.27	+25.0
+45	-50	-47.7	-2.27	+25.0
-45	-50	-47.7	-2.27	-25.0

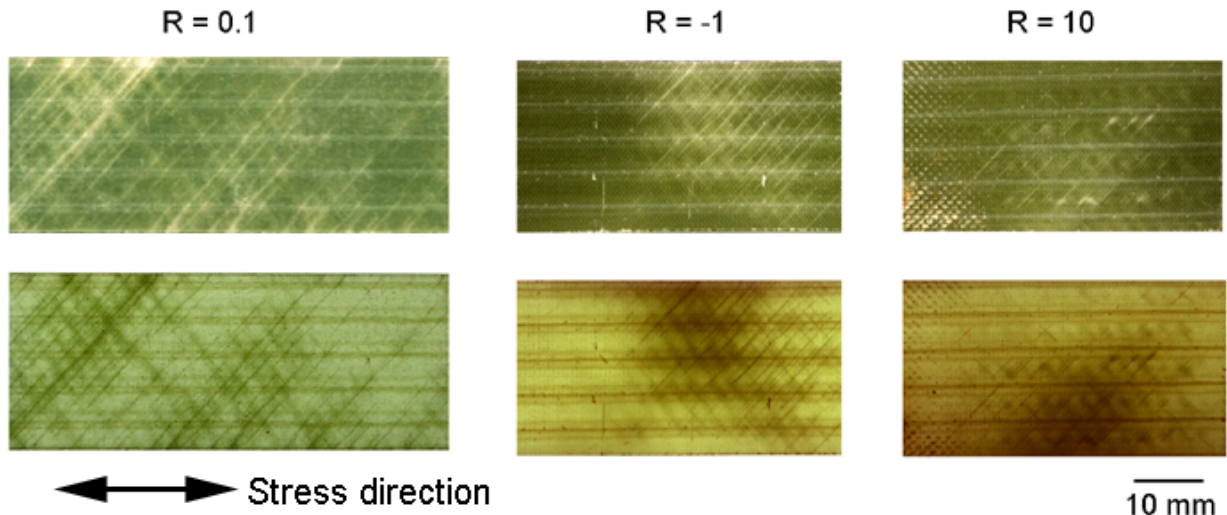


Figure 6. Matrix cracking at three R-values in reflected light (top) and transmitted light, fabric P laminates.

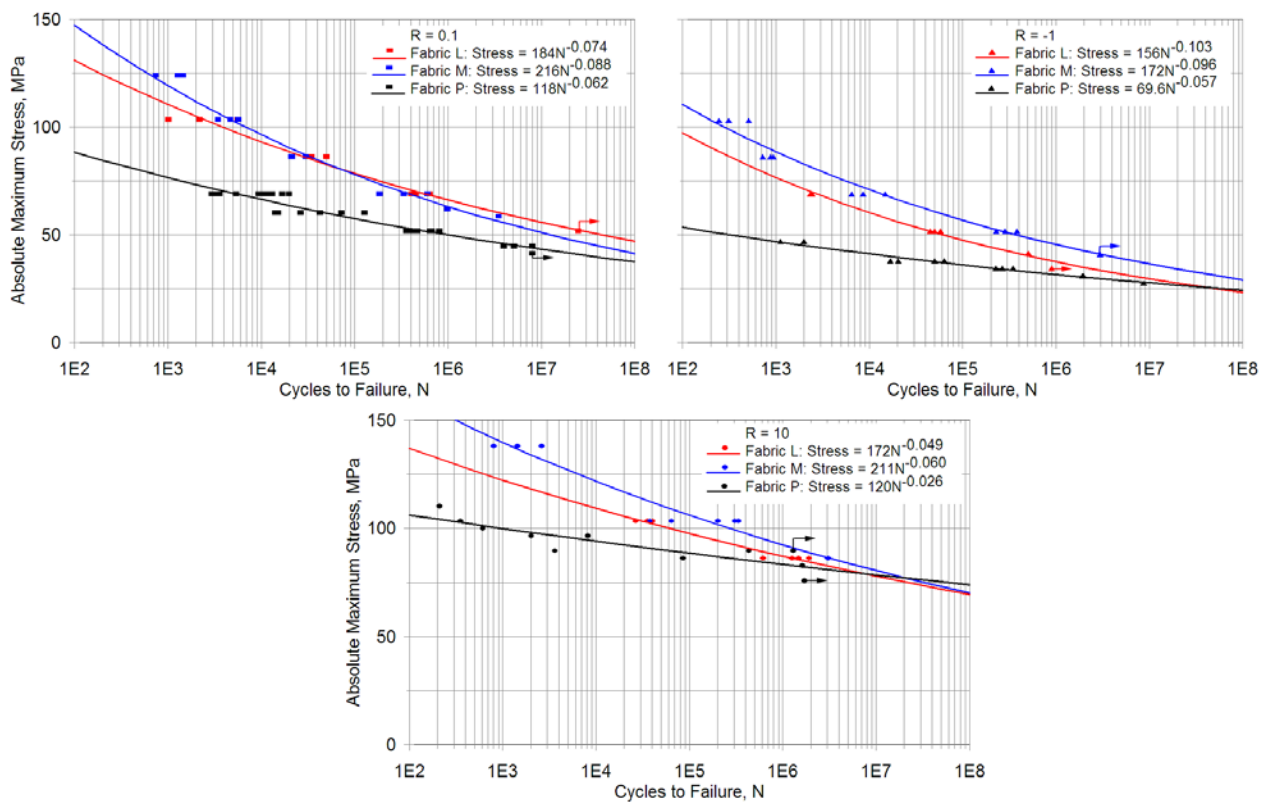


Figure 7. Maximum absolute stress vs. log cycles to failure for R = 0.1 (top left), -1.0 (top right) and 10 (bottom) for fabrics L, M and P.

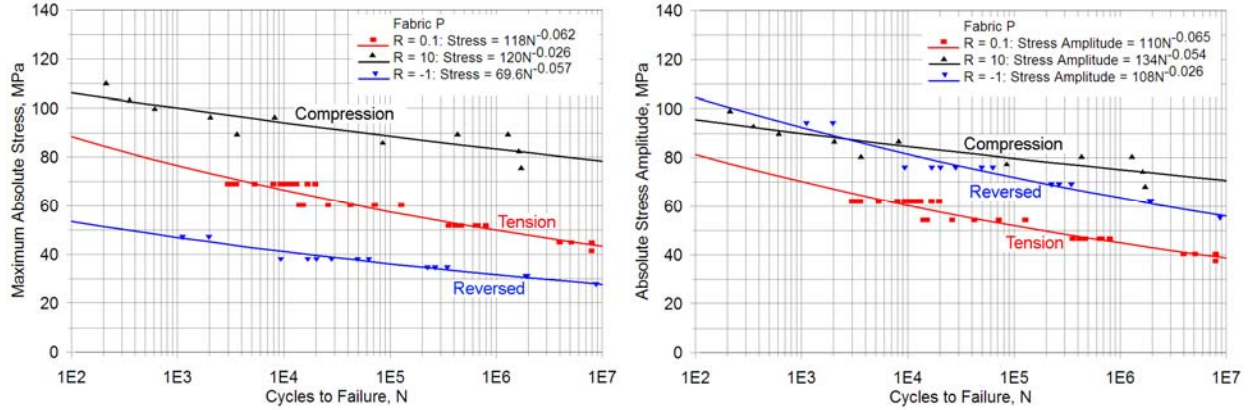


Figure 8. Comparison of maximum stress (left) and stress amplitude (right) S-N plots for fabric P laminates at $R = 0.1, -1$ and 10 .

Under reversed loading the shear and transverse tension stresses reverse in direction as the load changes from tension to compression; the failure mode was discussed earlier as related to local temperature rise resulting from damage and the large strain amplitude and hysteresis (shown later). The magnitude of the transverse stresses is low for this material relative to the shear stresses, but the static and fatigue responses are significantly different under tensile versus compressive loading (Figures 7 and 8). Van Paepegem, et al., provide detailed experimental characterization²³ and modeling²⁴ of the nonlinear stress-strain response of ± 45 glass/epoxy laminates.

C. Cyclic Creep and Stiffness Change

Stress-strain changes during load controlled cycling (Figure 9, top) reflect both a cyclic creep effect, with the coupon lengthening appreciably in tension or shortening in compression as cycles accumulate and both max and min strains increase, and a significant reduction in stiffness, indicated by a tilting to lower slope of the individual loops, most notable for $R = 0.1$ and -1 . The stiffness is calculated as (max-min) absolute stress/(max-min) absolute strain for an individual cycle. Plots of the average strain and the strain range vs. cycles are given in Figure 10 for typical tests of similar lifetime at each R -value. The average strain and strain range for particular cycles can be taken as measures of the creep strain and stiffness change, respectively¹⁵. The creep strain increases steadily for the $R = 0.1$ and 10 coupons, more rapidly toward the end for 0.1 ; much lower creep strain is present for $R = -1$ over most of the lifetime. The strain range, proportional to the stiffness, does not change significantly for compression (consistent with the residual stress-strain curve given later), but increases in the last decade for tension and reversed loading. Tamuzh, et al.¹⁵ attribute the stiffness change to cyclic damage effects which are independent of viscoelastic (creep) response, for off-axis laminates. Thus, the $R = 10$ response appears to be entirely dominated by creep, while the $R = 0.1$ and -1 responses show significant stiffness change associated with cyclic effects in the last decade, as well as significant creep strain for 0.1 . The fatigue exponents (Figure 8) are similar for $R = 0.1$ and -1 , but much lower for 10 .

Plots of maximum absolute strain for varied stress levels at each R -value in Figure 11 indicate maximum strains reaching several per cent in most tests before failure, with reduced strains at the lowest stresses and under reversed loading. The max strain typically increases by many times the initial max strain before failure. These figures indicate that very substantial strains accumulate for $R = 0.1$ and 10 before the stiffness decreases appreciably. Reversed loading produces smaller creep strains.

(It has been the practice in the past to report only the initial strains for the first few cycles for fatigue of ± 45 laminates in the database and reports^{1,9,10}, but these values have little meaning in characterizing test conditions, as evident from the results in this paper. However, for fiber dominated laminates, strain and stiffness changes are small⁵, and initial strains, while approximate in terms of cyclic conditions, provide simple and useful information.)

Strain controlled fatigue produced markedly different response, Figure 9 (bottom). For tensile fatigue (run with the thicker coupons to withstand compressive stresses), stress-relaxation at the higher strains on the first and subsequent cycles reduces the peak stress; the stiffness is not changed early in the lifetime, so the unloading strain excursion produces a compressive minimum stress. As cycling continues, the loop bottoms stabilize, but the stiffness now steadily decreases, lowering the maximum stress further. Compression loading in strain control produces changes

which are the inverse of those for tension, Figure 9, bottom right compared with bottom left, as the loop bottoms relax and the tops progress into tension. Under reversed loading at lower maximum strains, ($R = -1$, center bottom, Figure 9), the loops drift in a positive (tensile) direction similar to those for compression.

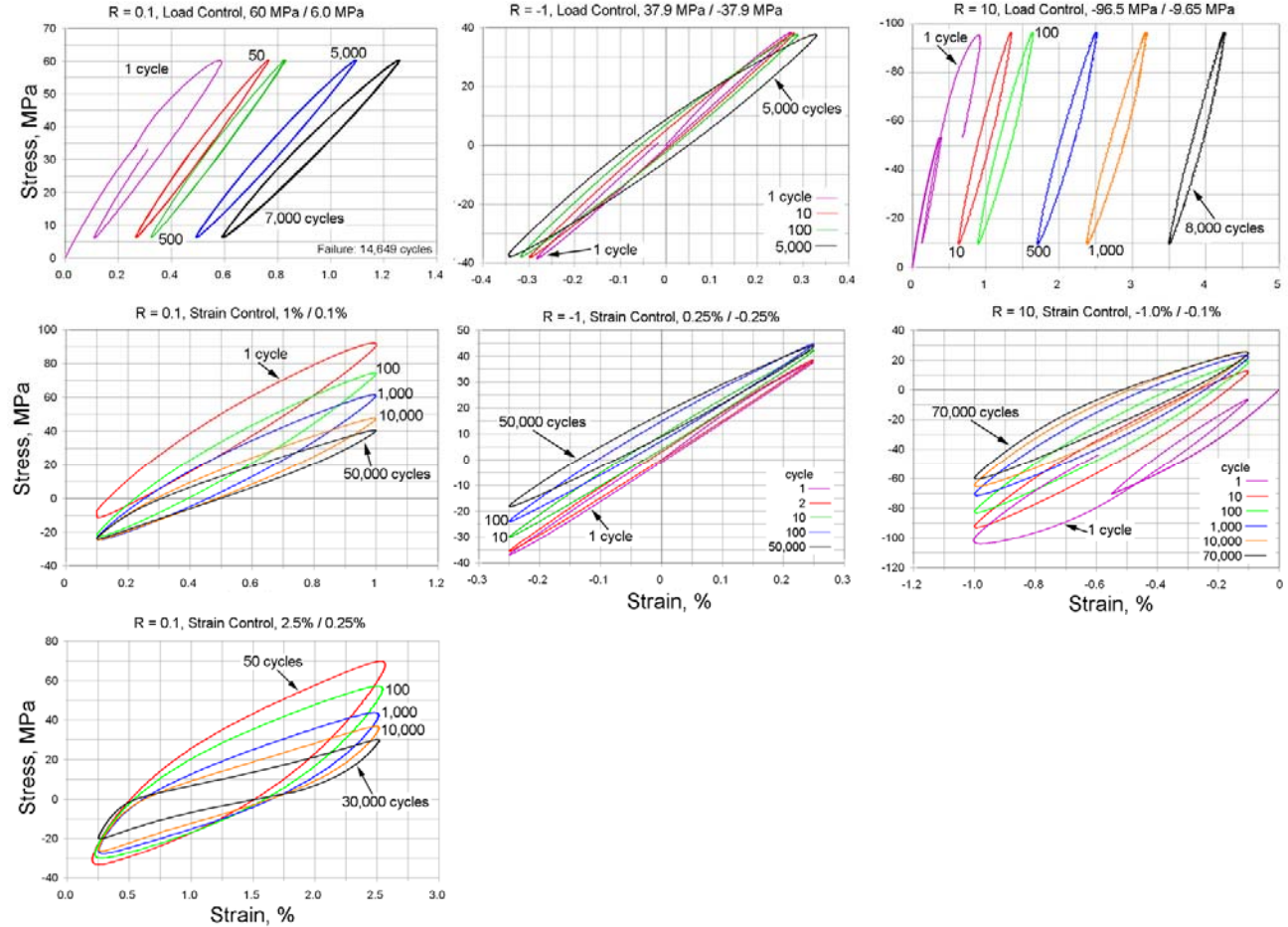


Figure 9. Typical cyclic stress-strain hysteresis loops for load control (top) and strain control (middle and bottom), fabric P, strain based $R = 0.1$ (left), -1 (center) and 10 (right).

D. Residual Stress-Strain

Cycles to complete failure for the $R = 0.1$, 60 MPa max load control case ranged from 10,000 to 100,000 cycles (Fig. 8). Selected coupons were cycled at $R = 0$ (for simplicity) to 4,000 and 10,000 cycles, then immediately tested for residual tensile stress-strain curve. Similarly, in compression fatigue, a coupon was cycled at $R = 10$, max abs stress of 96.5 MPa, with an expected lifetime around 10,000 cycles; the residual compressive stress-strain curve was determined on cycle 8,642. Stress-strain loops and the residual stress-strain curves are given in Figure 12. The residual stress-strain curves are compared with the virgin stress-strain curves in Figure 13, by offsetting the residual curves to zero strain by the amounts shown. The offset residual tensile stress-strain curve at 10,000 cycles is dramatically softened at most strains, but the maximum stress reached is only slightly reduced, relative to the virgin tensile stress-strain curves; less softening is evident for the 4,000 cycle tensile case. The offset residual compression curve shows no modulus change up to moderate stress, consistent with the absence of stiffness change discussed earlier, increased stiffness at high stress, and reduced maximum strain (by about the offset amount) relative to the virgin stress-strain curves. These limited cases show no significant decrease in residual ultimate strength, but more comprehensive testing for residual strength of similar ± 45 laminates has shown a steady decrease in tensile residual strength and stiffness after tensile fatigue loading; compressive residual strength is not found to decrease in a steady manner regardless of the fatigue loading condition⁵. The results in Figures 12 and 13 provide increased detail of changes to the stress-strain response as a result of cyclic loading for typical cases.

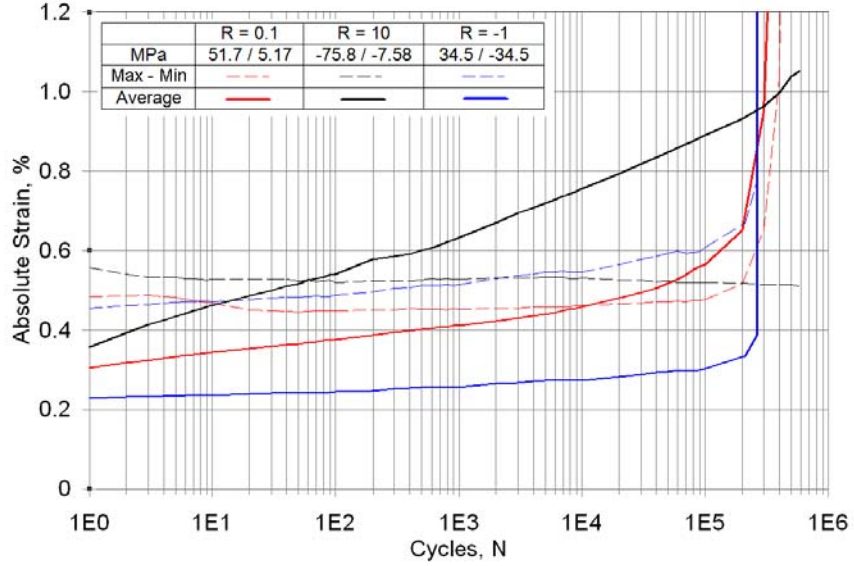


Figure 10. Typical individual test average strain, $(\text{max} + \text{min})/2$, and strain range $(\text{max}-\text{min})$ at each R-value.

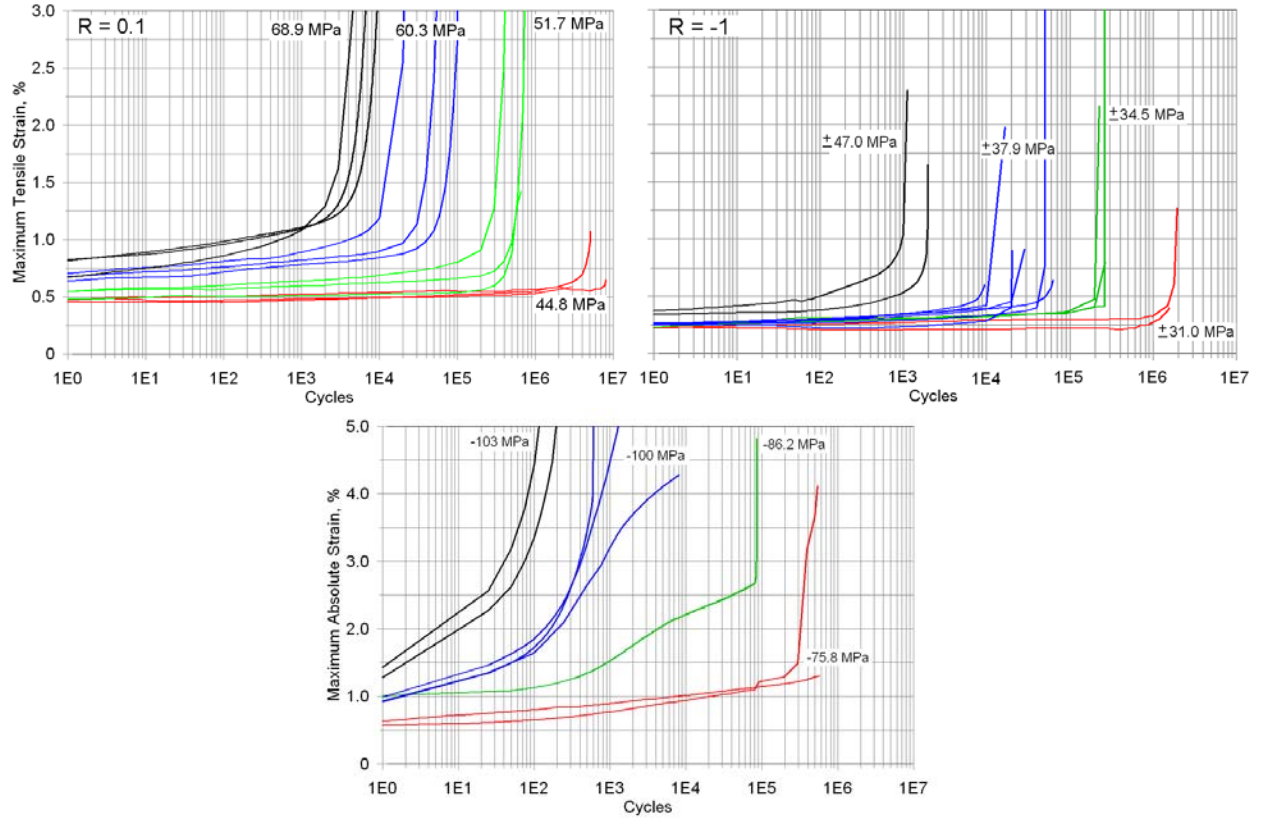


Figure 11. Maximum running strain over lifetime at different max loads, $R = 0.1$ (top left), -1 (top right) and 10 (bottom).

E. Damage Metric Comparisons

Different damage metrics are compared for fabric P laminate fatigue curves at each R-value in Figure 14. Total fatigue failure results are compared to cycles for a 25% decrease in stiffness (slope of the cyclic stress-strain loop) and a 50% increase in cumulative max abs strain. The 50% max strain metric is selected since it approximates the

point of rapid upturn on the max strain plots in Figure 11. The max strain, as opposed to the average, or creep, strain or stiffness, is viewed as potentially important in load transfer to adjacent UD structure, as discussed later. For $R = 0.1$ and -1 , individual tests reach the 50% max strain increase first, followed by the 25% stiffness loss and then total failure over most of the stress range. At the lowest stresses the $R = -1$ data tend to converge to a similar lifetime for the 25% stiffness change and failure, with the 50% strain increase not achieved in some cases; these are the conditions (reversed loading, initial strains below 0.25%) most likely to be approached in service loading for biaxial laminates in blades. In compression, $R = 10$, the 25% stiffness reduction is not reached before creep strains accumulate sufficiently (several %) to constitute failure. The 50% strain increase condition is reached much earlier than the failure condition in compression.

In choosing a failure condition for design purposes, a cumulative strain condition like 50% increase may be appropriate for compression, and occurs at much lower cycles than failure (Figure 14). Strain increase may also be appropriate at $R = 0.1$ for higher loads, shifting to stiffness change or failure at lower loads/longer lifetime. Stiffness change and failure lifetimes are similar at $R = -1$. Only the reversed loading tests approach the low strain levels at failure which might be realized for blades in service, and there the stiffness change and failure cycles tend to converge. However, creep strains can reach the 50% increase range at similarly low stresses, as discussed next.

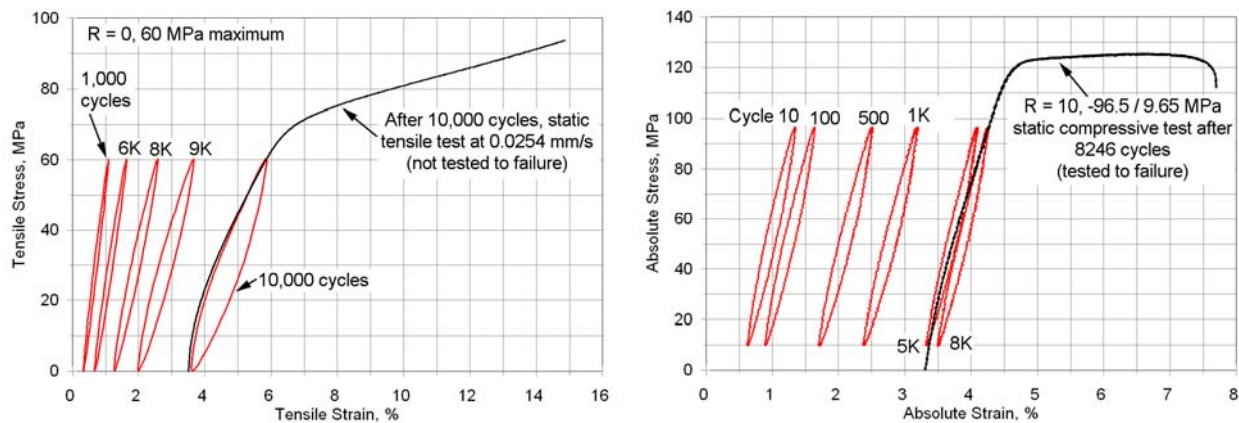


Figure 12. Left, coupon tested at $R = 0$ (0-tension), max stress 60 MPa, stress-strain loops with residual tensile stress-strain test immediately after cycle 10,000; right, compression loops, $R = 10$, max abs stress 96.5 MPa, with residual compressive stress-strain curve after cycle 8,246.

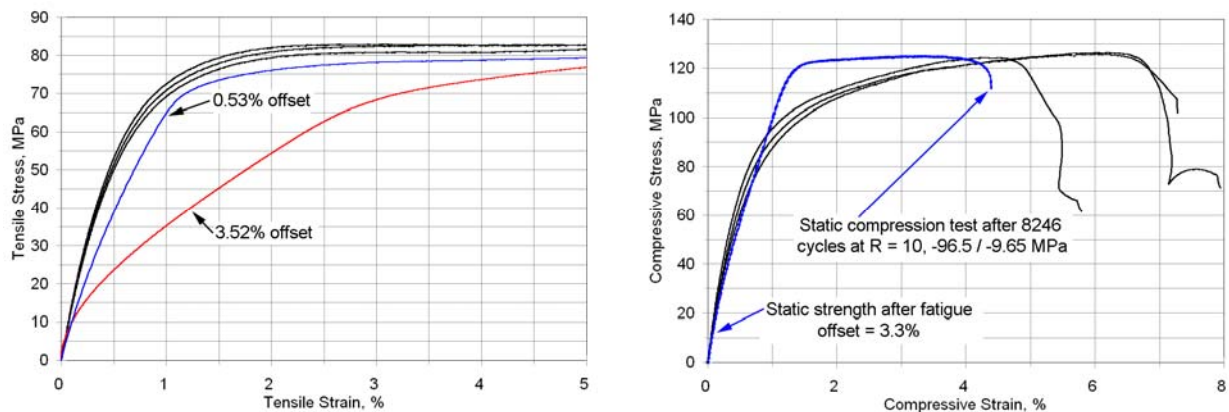


Figure 13. Comparison of virgin stress-strain curves (black) with residual stress-strain curves: left, $R = 0$, 60 MPa max, after cycle 4,000 (blue, 0.53% strain offset) and 10,000 (red, 3.52% strain offset); right, $R = 10$, -96.5 MPa max, after cycle 8246, 3.3% strain offset.

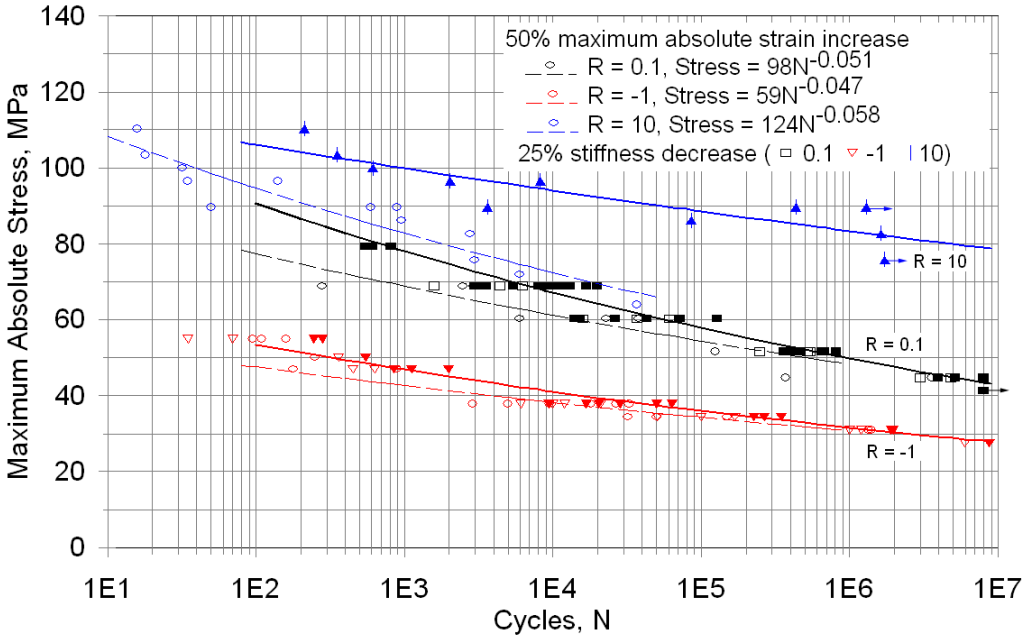


Figure 14. Data for 25% stiffness decrease and 50% max absolute strain increase plotted against failure S-N curves from Figure 10.

F. Creep and Cyclic Loading Comparison

Creep test results for various tensile and compressive stresses are given in Figure 15. These tests were not taken to failure, but are intended to define the time at the 50% strain increase condition. Even at the lowest abs stress, 38 MPa, the strain accumulates to the 50% increase condition in about 10^5 seconds, just more than one day. The only results at the same absolute stress, 60 MPa, in both tension and compression, show very similar creep strains for both. Thus, while the cyclic lifetimes for $R = 0.1$ and 10 differ significantly (Figure 8), the creep response in tension and compression is very similar, reflecting the dominance of the ply shear stresses, which have identical magnitudes in each case (Table 2). The difference under cyclic loading appears to relate to the decreasing stiffness with damage in the last decade of cycles in tension, but nearly constant stiffness in compression (Figure 10).

A comparison of the cumulative test times to reach the 50% max strain condition for creep vs. cyclic tests in tension and compression is given in Figure 16. While there is significant scatter, all of the cases show similar times to 50% strain increase, and similar trends with stress. The creep conditions reach 50% strain increase before the cyclic conditions at most stresses. Sine wave fatigue loading results in only a brief time near max load on each cycle compared to the square wave loading illustrated in Figure 2, and the cumulative time at max load is difficult to define; this may cause the slightly longer cumulative total test times in fatigue.

G. Effects of 0°-Ply Addition to Biaxial Laminate

The effect of adding UD plies to the biax laminates is illustrated in Figure 17 for a $[(\pm 45)_3/0/(\pm 45)_3]_S$ laminate. While UD laminates show minimal max strain increases before fiber failure⁵, interactions with biaxial plies in adjacent structure or within MD laminates like this, can result in significant load transfer onto the UD plies as biaxial plies creep and accumulate damage. The test result illustrated in Figure 17 for a laminate with 20% UD fabric (PPG-Devold 1200L/G30-E07) shows the steady stiffness loss and creep associated with the biaxial laminates with an initial strain around 0.8%, but the rate of max strain increase and softening is much reduced compared to an all-biaxial laminate, such as Figure 11, $R = 0.1$, 68.9 MPa. Deformation in the biaxial plies is restricted by the higher modulus 0° plies. As the biaxial plies soften and creep, the stress and strain on the 0°-plies increases until they fail, one after another (the strain is the same in all plies). The lifetime for an all UD laminate with this fabric and resin is reported^{2,6} as about 10^6 cycles for an initial max strain around 0.80%, falling to about 10^5 cycles for an initial max strain of 1.25%; these strains represent the first and 100,000th cycles in Figure 17. Thus, the creep and softening of the biaxial plies before failure of the 0° plies results in an apparent decrease of a factor of ten in lifetime, at least for this single coupon, but consistent with other tests and literature observations⁵.

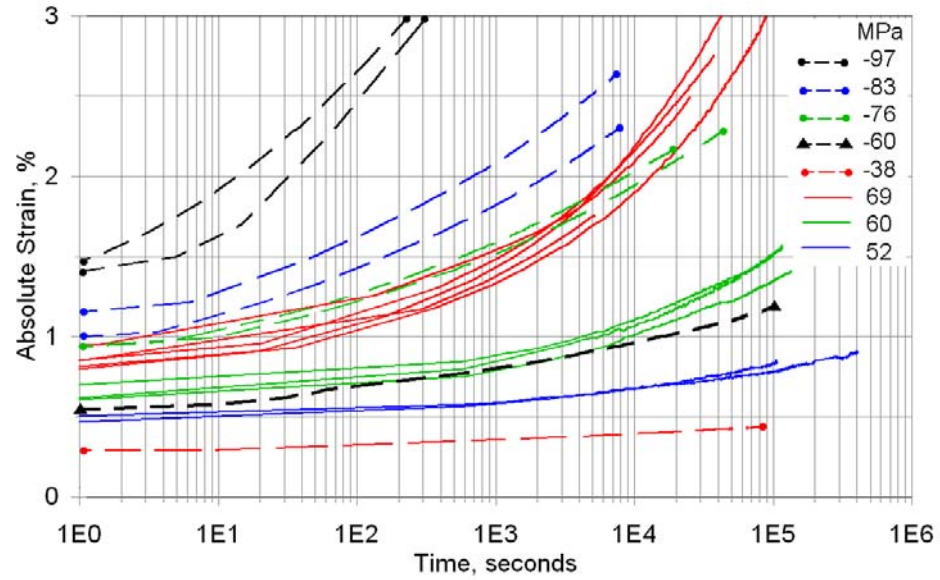


Figure 15. Creep strain vs. time for tension and compression, not taken to failure.

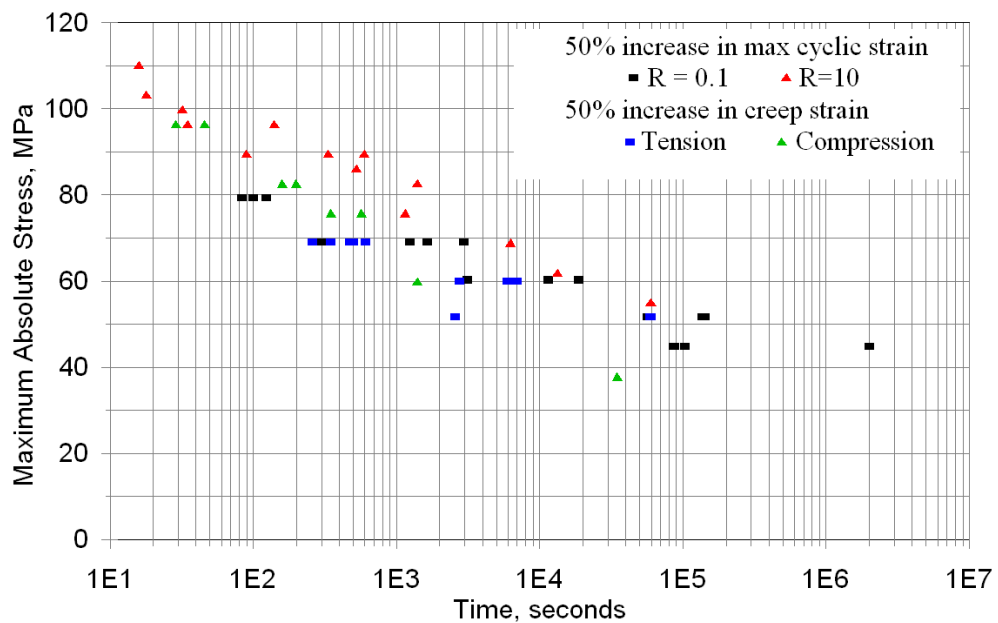


Figure 16. Cumulative test time to reach 50% increase in max strain at different max stresses for tensile and compressive creep, compared with fatigue at $R = 0.1$ and 10.

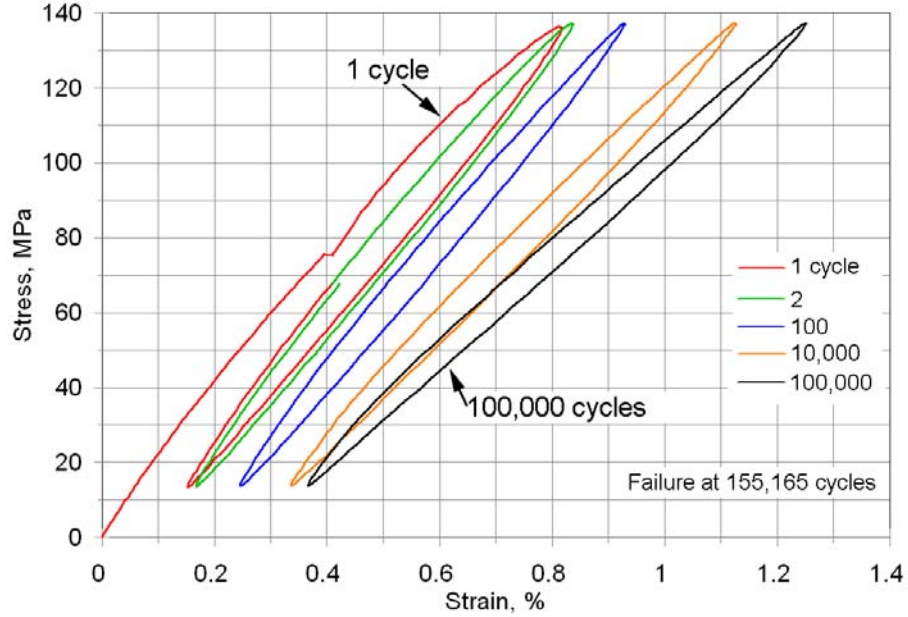


Figure 17. Cyclic stress-strain loops for laminate containing 25% 0° fibers, coupon tested at R = 0.1, 138 MPa max stress, failure at 155,165 cycles.

IV. Conclusions

The results of this exploratory experimental study indicate the importance of creep response in the cyclic fatigue of infused biaxial glass fabric (± 45) reinforced epoxy laminates typical of wind blade shells and webs. The following are the main conclusions:

1. Both the static and S-N fatigue strengths are significantly greater in compression than tension (Figures 5 and 8). Reversed loading results in the lowest S-N trend when max stress based, but the stress amplitude S-N trend is similar to compression (Figure 8). Fabric P laminate S-N trends at all three R-values fall below those for fabrics L and M, which have different backing, fiber content and cure conditions.
2. Compression fatigue is creep dominated, with little stiffness change. Tension and reversed loading fatigue show similar fatigue exponents and a significant decrease in stiffness associated with cyclic effects in the last decade of cycles. However, tensile fatigue may be creep limited in applications over much of the stress range, even though the final failure is cycle dominated at lower stresses. Stiffness change, creep and failure cycles converge at the lowest stresses for R = -1, which may approach some blade service conditions.
3. Cumulative test times to reach an increase of 50% in the max strain, over a range of stresses, are similar for creep and fatigue, and for tension and compression.
4. The addition of 20% 0-degree UD plies to a biaxial laminate under tensile fatigue results in a sequence of creep and softening of the biaxial plies, but at a reduced rate due to the constraint of the UD plies. The strain increases in the UD plies as the biaxial plies soften, until the UD plies eventually fail at a lifetime which is reduced by about a decade compared with the expected lifetime at the initial strain.
5. Testing under controlled strain conditions as would occur with a high per cent of 0° plies, or adjacent UD structure, results in increased lifetime and stabilized stress-strain loops shifted toward compression for R = 0.1 and tension for R = -1 and 10.

Acknowledgements

This research was supported by Sandia National Laboratories, Joshua Paquette, technical manager. The support and encouragement of the many industry materials suppliers is greatly appreciated.

References

- ¹Mandell, JF, Samborsky, DD, Agastra, P, Sears, AT and Wilson, TJ, "Analysis of SNL/MSU/DOE Fatigue Database Trends for Wind Turbine Blade Materials," Sandia Contractor Report SAND2010-7052 (www.coe.montana.edu/composites/).
- ²Samborsky, DD, Agastra, P and Mandell, JF, "Fatigue Trends for Wind Blade Infusion Resins and Fabrics," 2010 AIAA SDM, Orlando, AIAA-2010-282.
- ³Mishnaevsky, L, Brondsted, P, Nijssen, R, Lekou, DJ and Philippidis, TP, "Materials of large wind turbine blades: recent results in testing and modeling," *Wind Energy*, 15, 2011 83-97.
- ⁴Philippidis, TP and Vassilopoulos, AP, "Fatigue of composite laminates under off-axis loading," *Int. J. Fatigue*, 1999, no. 21, pp.253-262.
- ⁵Philippidis, TP and Eliopoulos, EN, "Verified material model incorporating progression of damage due to static loading and the effect of fatigue on residual strength and stiffness," 2011 (www.upwind.eu/media/732/Deliverable_D3_3_4).
- ⁶Samborsky, DD, Sears, AT, Agastra, P and Mandell, JF, "Mixed Mode Static and Fatigue Crack Growth in Wind Blade Paste Adhesives," 2011 AIAA SDM Conference, Denver, AIAA-2011-1755.
- ⁷Samborsky, DD, Mandell, JF and Miller, D, "The SNL/MSU/DOE fatigue of composite materials database: recent trends," 2012 AIAA SDM conference, Honolulu, AIAA-2012-1573.
- ⁸Kensche, C, "Final report on tube testing," Optimat Blades OB_TG2_R038 rev. 0, 2006 (www.wmc.eu/optimatblades.php).
- ⁹Mandell, JF, Samborsky, DD and Cairns, DS, "Fatigue of Composite Materials and Substructures for Wind Turbine Blades," Contractor Report SAND2002-0771, Sandia National Laboratories, Albuquerque, NM, 2002.
- ¹⁰Mandell, JF and Samborsky, DD, "DOE/MSU Fatigue of Composite Materials Database, 2012 update (www.sandia.gov/wind/other/973002upd0309.pdf).
- ¹¹Shapery, RA, "Viscoelastic behavior and analysis of composite materials," in *Mechanics of Composite Materials*, Vol.2, G. P. Sendeckyj, ed., Academic Press, New York, 1974.
- ¹²Tuttle, ME and Brinson, HF, "Prediction of long term creep compliance of general composite laminates," *Experimental Mechanics*, 1985 89-102.
- ¹³Kawai, M, "Constitutive modeling of viscoplastic deformation of polymer matrix composites," in *Creep and Fatigue in Polymer Matrix Composites*, R. Guedes, Ed., Woodhead, Cambridge UK, 2011, 492-511234-272.
- ¹⁴Gates, TS, Veazie, DR and Brinson, LC, "A comparison of tension and compression creep in a polymeric composite and the effects of physical aging on creep," NASA Technical Morandum 110273, August, 1996.
- ¹⁵Tamuzh, V, Andersons, J, Aniskevich, K, Jansons, J and Korsgaard, J, "Creep and damage accumulation in orthotropic composites under cyclic loading," *Mechanics of Composite Materials*, 34, 1998, 321-330.
- ¹⁶Mandell, JF and Meier, U, "Effects of stress ratio, frequency and loading time on the tensile fatigue of glass-reinforced epoxy," *Long Term Behavior of Composites, ASTM STP 813*, T. K. O'Brien, Ed., ASTM, Phil., 1983, pp. 55-77.
- ¹⁷Nijssen , R, Stammes, E and Westphal, T, "Material and subcomponent research for improved rotor blade design," Second Technical Conf. on Wind Turbine Rotor Blades, Essen, Germany, June, 2010.
- ¹⁸Raijmaekers, ., Westphal, T, Stammes, E and Nijssen, R, "Effect of temperature and frequency on fatigue life: literature study and tension fatigue experiments," Proc. EWEA, 2009.
- ¹⁹Epaarachchi, JA, "The effect of viscoelasticity on fatigue behavior of polymer matrix composites," in *Creep and Fatigue in Polymer Matrix Composites*, R. Guedes, Ed., Woodhead, Cambridge UK, 2011, 492-511.
- ²⁰Mandell, JF, Reed, RM Jr and Samborsky, DD, "Fatigue of Fiberglass Wind Turbine Blade Materials," Contractor Report SAND92-7005, Sandia National Laboratories, Albuquerque, NM (1992).
- ²¹"OptiDAT Fatigue of Wind Turbine Blade Materials Database," (www.wmc.eu/optimatblades_optidat.php).
- ²²Daniel, IM and Ishai, O, *Engineering Mechanics of Composite Materials*, Oxford Univ. Press, Oxford, 1994, 106-109.
- ²³Van Paepegem, W, De Baere, I, and Degrieck, J, "Modeling the nonlinear stress-strain response of glass fibre-reinforced composites. Part I: Experimental Results," *Comp Sci Techn*, 66 (2006), 1455-1464.
- ²⁴Van Paepegem, W, De Baere, I, and Degrieck, J, "Modeling the nonlinear stress-strain response of glass fibre-reinforced composites. Part II: model development and finite element simulations," *Comp Sci Techn*, 66 (2006), 1465-1478.